

Pressure induced phase transition of ZrN and HfN: a first principles study

A. T. Asvini Meenaatci^a, R. Rajeswarapalanichamy^{a,*}, and K. Iyakutti^b

^a Department of Physics, N. M. S. S. Vellaichamy Nadar College, Madurai,
Tamilnadu-625019, India

^b Department of Physics and Nanotechnology, SRM University, Chennai,
Tamilnadu-603203, India

Received 10 December 2012; Accepted (in revised version) 20 January 2013

Published Online 30 August 2013

Abstract. The structural, elastic, and electronic properties of zirconium nitride (ZrN) and hafnium nitride (HfN) are investigated by first principles calculation with density functional theory. The obtained cubic NaCl structure is energetically the most stable structure at ambient pressure. A pressure induced structural phase transition from B1 to B2 phase is predicted. The estimated superconducting transition temperature (T_c) of ZrN and HfN are 9.17 K and 8.66 K respectively. As pressure increases the superconducting transition temperature also increases.

PACS: 31.15.A-,62.20.D-, 61.50.Ks, 74.70.Ad

Key words: electronic structure, elastic properties, structural phase transitions, superconducting transition temperature

1 Introduction

The physical properties of materials undergo a variety of changes when subjected to high pressure [1]. The increase of pressure means the significant decrease in volume, which results in the change of electronic states and crystal structure. The recent developments in diamond anvil cell [2] enable the experimentalist to perform the investigation at high pressure. With the development of high pressure experimental techniques, investigations on pressure induced structural phase transition and superconductivity are getting the attention of all.

Transition metal nitrides ZrN and HfN are of great technological and fundamental importance because of their strength and durability as well as their useful optical, electronic, magnetic and superconducting properties. The technological application of all

*Corresponding author. *Email address:* rajesarapalanichamy@gmail.com (R. Rajeswarapalanichamy)

the above compounds requires significant progress in the fundamental understanding of their behavior at normal and high pressures. At ambient pressure both ZrN and HfN crystallize in the NaCl structure. Recently Chen *et al.* [3], using zone annealing technique grown hafnium nitride (HfN) and zirconium nitride (ZrN) crystals in the rock salt structure and they were identified as superconductors at ambient pressure. The measured bulk modulus was 215 GPa (ZrN) and 306 GPa (HfN) by neutron scattering experiments. There are many theoretical as well as experimental investigations on the structural stability ZrN and HfN [4-11]. But there are many disagreements between the theory and experiments in the prediction of stable structure, equilibrium lattice constant and bulk modulus of these transition metal nitrides TMNs (TM-Zr, Hf). This necessitated further theoretical studies in these systems. Moreover, the pressure dependence of elastic moduli and superconductivity have not been reported yet.

In the present investigation, the electronic structure, structural phase transition and mechanical stability of ZrN and HfN have been investigated using Vienna ab-initio simulation package (VASP) for all possible cubic and hexagonal structures. The superconducting transition temperature is also estimated using tight binding linear muffin tin orbital (TB-LMTO) method.

2 Computational details

The total energy calculations are performed in the frame work of density functional theory using the generalized gradient approximation (GGA) [12-14] as implemented in the VASP code [15-17]. Ground-state geometries are determined by minimizing stresses and Hellman-Feynman forces using the conjugate-gradient algorithm with force convergence less than 10^{-3} eV Å⁻¹. Brillouin zone integration is performed with Gaussian broadening of 0.1 eV during all relaxations. The wave function of the valence electron is expanded by a plane wave basis with an energy cutoff of 600 eV, which is tested to be fully converged with respect to the total energy for many different volumes. Brillouin-zone integrations are performed using the Monkhorst-Pack scheme [18] with a grid size of $12 \times 12 \times 12$ for structural optimization. A similar density of k-points and energy cut-off are used to estimate total energy as a function of volume for all the structures considered for the present study. Scalar-relativistic corrections are also included in all the calculations. Iterative relaxation of atomic positions is stopped when the change in total energy between successive steps is less than 1 meV/cell. With this criterion, the force on the atoms is generally less than 0.1 eV/Å.

To search for the most stable structure of the transition metal nitrides TMNs (TM=Zr, Hf), 5 types of the potential structures have been considered. They include NaCl (B1), Zinc blende (ZB)(B3), CsCl (B2), WC(Bh) and NiAs(B8). The space group and atomic position of atoms in the five different phases of TMNs are tabulated in Table 1. The electronic configurations of Zr, Hf and N atoms are [Kr] 4d²5s² (Z=40), [Xe] 4f¹⁴5d²6s² (Z=72), and [He] 2s²2p³ (Z=7) respectively. The valence electronic configurations chosen

Table 1: The space group and atomic position in the five phases of TMNs (TM- Zr, Hf).

| Phase | Space group | Atomic position | |
|----------|----------------------|-----------------|--------------------|
| | | TM | N |
| WC (Bh) | P6-m2 | 0, 0, 0 | 0.333, 0.667, 0.5 |
| NiAs(B8) | P6 ₃ /mmc | 0, 0, 0 | 0.333, 0.667, 0.25 |
| NaCl(B1) | Fm3-m | 0, 0, 0 | 0.5, 0.5, 0.5 |
| CsCl(B2) | Pm3-m | 0, 0, 0 | 0.5, 0.5, 0.5 |
| ZB(B3) | F4-3m | 0, 0, 0 | 0.25, 0.25, 0.25 |

in our calculation are $4d^25s^2$ for Zr, $5d^26s^2$ Hf and $2s^22p^3$ for N atoms.

The unit cell for all the structures of TMNs is shown in Fig. 1.

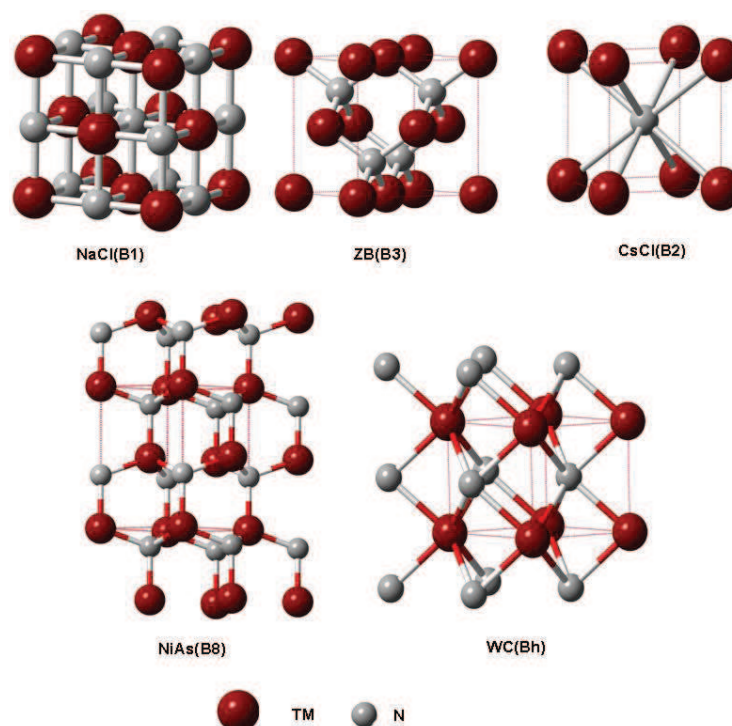


Figure 1: Unit cell of various phases of Transition metal nitrides TMNs (TM- Zr,Hf).

The tight binding linear muffin tin orbital method [19-20] was used for the estimation of electron- phonon coupling constant and electron-electron interaction parameter. Von-Barth and Hedin parameterization scheme is used for exchange correlation potential. The Wigner-Seitz sphere was chosen in such a way that the boundary potential was minimum and charge flow between the atoms was in accordance with the electro-negativity criteria. The E and K convergence are also checked. The tetrahedron method [21] of Brillouin zone

integration is used to calculate the total density of states.

3 Results and discussion

3.1 Structural stability and ground state properties

In order to calculate the ground state properties of ZrN and HfN, the total energies are calculated for five possible phases (B1, B2, B3, Bh and B8) with different reduced volumes. Fig. 2 (a-b) indicates the plot of the calculated total energy versus reduced volume for ZrN and HfN respectively.

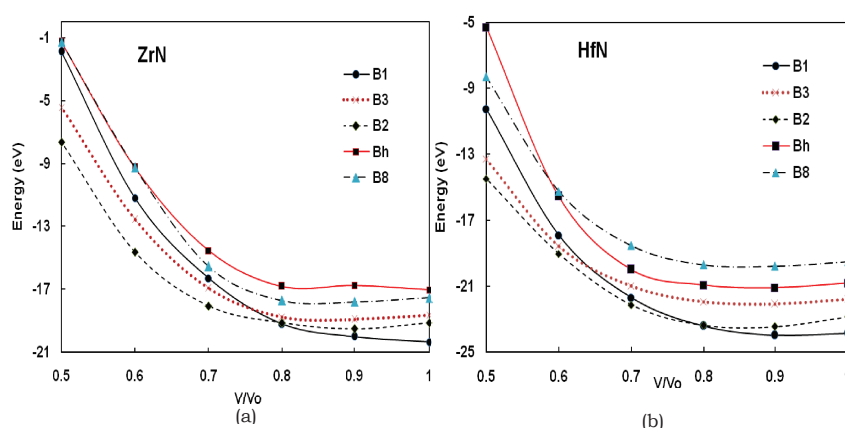


Figure 2: Total energy versus reduced volume variations for five different crystallographic structures of: (a) ZrN, (b) HfN.

From these figures, it is observed that both ZrN and HfN are highly stable in the B1 phase at normal pressure, which is consistent with the experimental and other theoretical reports. The calculated total energies are fitted to the Birch Murnaghan equation of state (EOS) [22] to determine the ground state properties such as equilibrium lattice constant and cell volume. The calculated volume $V_0(\text{\AA}^3)$, lattice parameters a and c (\AA), TM-N bond length (\AA), c/a ratio, valence electron density ρ (electrons/ \AA) obtained using VASP code are given in Table 2, along with experimental [3-4,10] and theoretical [5-9,11] results. From the Table 2, it is observed that the calculated lattice constants are in good agreement with the experimental and previous theoretical results.

From Fig. 2 (a-b), it is also observed that both ZrN and HfN will undergo a structural phase transition from B1 to B2 phase under pressure. In order to determine the transition pressure at $T=0$ K, the enthalpy (H) is calculated using the expression, $H = E + PV$. The stable structure at a given pressure is the structure for which the enthalpy has its lowest value. The transition pressure corresponding to the phase transition from B1 to B2 phase is obtained from the relation $H_{B1}(P) = H_{B2}(P)$, where H_{B1} and H_{B2} are the enthalpies

Table 2: Calculated lattice parameters a and c (Å), cell volume V_0 (Å³), the shortest TM-N bond distance (Å), Valence electron density ρ (electrons/Å³) and c/a ratio at the GGA level for five different phases of ZrN and HfN.

| | ZrN | | | | | HfN | | | | |
|--------|-------------------|--------------------|--------------------|--------------------|-------------------|---------------------|-------|-------|-------|-------|
| | B1 | B2 | B3 | Bh | B8 | B1 | B2 | B3 | Bh | B8 |
| V_0 | 23.98 | 23.89 | 30.48 | 24.65 | 24.28 | 24.11 | 23.76 | 31.80 | 23.79 | 23.66 |
| | 23.9 ^d | 22.83 ^f | 30.58 ^f | 24.80 ^f | 24.9 ^g | 24.8 ⁱ | | | | |
| | 4.578 | 2.88 | 4.959 | 3.128 | 3.191 | 4.586 | 2.875 | 5.029 | 2.957 | 3.195 |
| a | 4.58 ^a | 2.473 ^e | 4.964 ^f | 3.132 ^f | 3.22 ^g | 4.52 ^{d,h} | | | | |
| | 4.57 ^b | | | | | 4.54 ^b | | | | |
| | 4.58 ^c | | | | | 4.627 ⁱ | | | | |
| c | | | | 2.91 | 5.308 | | | 2.844 | 5.353 | |
| | | | | 2.918 ^f | 5.34 ^g | | | | | |
| TM-N | 2.28 | 2.38 | 2.24 | 2.32 | 2.33 | 2.27 | 2.41 | 2.18 | 2.34 | 2.34 |
| | | | | | | 2.26 ^h | | | | |
| ρ | 0.375 | 0.376 | 0.295 | 0.367 | 0.370 | 0.373 | 0.373 | 0.283 | 0.378 | 0.380 |
| c/a | | | | 0.930 | 1.663 | | | | 0.961 | 1.675 |

^a Exp, Ref. [4].

^b FLAPW method within GGA, Ref. [5].

^c US-PP method within GGA, Ref. [6].

^d Exp, Ref. [3].

^e TBIPT, Ref. [7].

^f GGA, Ref. [8].

^g LDA, Ref. [9].

^h Exp, Ref. [10].

ⁱ GGA, Ref. [11].

of the B1 and B2 phases respectively. The enthalpy versus pressure curves for both the structures for ZrN and HfN are displayed in Fig. 3 (a-b).

The estimated transition pressure for ZrN and HfN is 98.53GPa and 134GPa, which is consistent with the transition pressure of Poonam Ojha *et al.* [7].

3.2 Elastic properties

Elastic constants are the measure of the resistance of a crystal to an externally applied stress. For small strains Hooke's law is valid and the crystal energy E is a quadratic function of strain [23]. Thus to obtain the total minimum energy for calculating the second order elastic constants, a crystal is strained and all the internal parameters are relaxed. Consider a symmetric 3×3 nonrotating strain tensor ε which has matrix elements ε_{ij} ($i, j = 1, 2$ and 3) defined by Eq. 1.

$$\varepsilon_{ij} = \begin{pmatrix} e_1 & \frac{e_6}{2} & \frac{e_5}{2} \\ \frac{e_6}{2} & e_2 & \frac{e_4}{2} \\ \frac{e_5}{2} & \frac{e_4}{2} & e_3 \end{pmatrix} \quad (1)$$

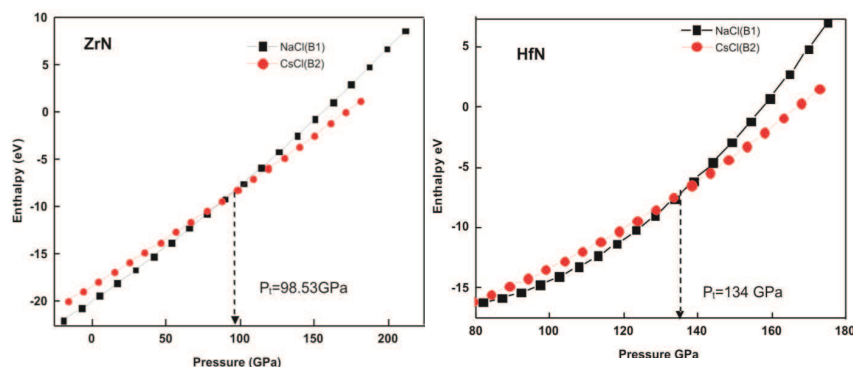


Figure 3: Enthalpy versus pressure curve for: (a) ZrN and (b) HfN in NaCl (B1) and CsCl (B2) structure.

such a strain transforms the three lattice vectors defining the unstrained Bravais lattice (a_K , $K=1,2$ and 3) to the strained vectors ($a_{K'}$, $K'=1,2$ and 3) as given by Eq. (2)

$$a'_{K'} = (I + \varepsilon)a_K \quad (2)$$

where I is defined by its elements, $I_{ij} = 1$ for $i = j$ and 0 for $i \neq j$. Each lattice vector a_k or $a'_{k'}$ is a 3×1 matrix. The change in total energy due to the above strain (1) is

$$\Delta E = \frac{E(\{e_i\}) - E_0}{V_0} = \left(1 - \frac{V}{V_0}\right)P(V_0) + \frac{1}{2} \left(\sum_1^6 \sum_1^6 C_{ij} e_i e_j \right) + O(\{e_i^3\}) \quad (3)$$

where V_0 is the volume of the unstrained lattice, E_0 is the total minimum energy corresponding to the unstrained volume of the crystal, $P(V_0)$ is the pressure of the unstrained lattice, and V is the new volume of the lattice due to strain in Eq. (1). In Eq. (3), due to crystal symmetry C_{ij} is equal to C_{ji} (i.e. $C_{ij} = C_{ji}$). This reduces the elastic constants from 36 to 21. Further crystal symmetry reduces the number to 5 (C_{11} , C_{12} , C_{44} , C_{13} , C_{33}) for hexagonal crystals and 3 (C_{11} , C_{12} , C_{44}) for cubic crystals. A proper choice of the set of strains e_i , $i = 1, 2, \dots, 6$, in Eq. (3) leads to a parabolic relationship between $\Delta E/V_0$ ($\Delta E \equiv E - E_0$) and the chosen strain. Such choices for the set $\{e_i\}$ and the corresponding form for ΔE are shown in Table 3 for cubic [24] and hexagonal [25] lattices.

For each lattice structure of ZrN and HfN studied, we strained the lattice by 0%, $\pm 1\%$, and $\pm 2\%$ to obtain the total minimum energies $E(V)$ at these strains. These energies and strains are fitted with the corresponding parabolic equations of $\Delta E/V_0$ as given in Table 3 to yield the required second-order elastic constants. While computing these energies all atoms are allowed to relax with the cell shape and volume fixed by the choice of strains $\{e_i\}$. From the calculated elastic constants C_{ij} , the bulk modulus and shear modulus of cubic and hexagonal crystals are calculated using the Voigt-Reuss-Hill (VRH) averaging scheme [26-28]. The strain energy $1/2 C_{ij} e_i e_j$ of a given crystal in Eq. (3) must always be positive for all possible values of the set $\{e_i\}$; otherwise the crystal would be mechanically unstable. The calculated elastic constants C_{ij} (GPa), bulk modulus B_0 (GPa) and its

Table 3: Strain combinations in the strain tensor [Eq.(1)] for calculating the elastic constants of cubic and hexagonal structures.

| Cubic crystals | | | Hexagonal crystals | |
|---|---------------------------------|------------------|--|--|
| Strain parameters | $\Delta E/V_0$ | Parameters | $\Delta E/V_0$ | |
| (unlisted $e_i=0$) | | | (unlisted $e_i=0$) | |
| 1 $e_1=e_2=\delta, e_3=(1+\delta)^{-2}-1$ | $3(C_{11}-C_{12})\delta^2$ | $e_1=\delta$ | $(1/2) C_{11}\delta^2$ | |
| 2 $e_1=e_2=e_3=\delta$ | $(3/2)(C_{11}+2C_{12})\delta^2$ | $e_3=\delta$ | $(1/2) C_{33}\delta^2$ | |
| 3 $e_6=\delta, e_3=\delta^2(4-\delta^2)^{-1}$ | $(1/2) C_{44}\delta^2$ | $e_4=\delta$ | $(1/2) C_{44}\delta^2$ | |
| 4 | | $e_1=e_2=\delta$ | $(C_{11}+2C_{12})\delta^2$ | |
| 5 | | $e_1=e_3=\delta$ | $(1/2)(C_{11}+C_{33}+2C_{13})\delta^2$ | |

Note: The independent elastic constants for cubic (B1,B2,B3 structures) and hexagonal (B8, Bh structures) are calculated from the above strains. Symmetry dictates $C_{ij}=C_{ji}$ and all unlisted $C_{ij}=0$. The strain δ is varied in steps of 0.01 from $\delta=-0.02$ to 0.02. ΔE [Eq. (3)] is the The equilibrium or unstrained lattice volume is V_0 .

derivative B'_0 , Young's modulus E (GPa), Shear modulus G (GPa), Poisson's ratio (ν), B/G ratio, elastic anisotropy A and micro hardness H (GPa) for ZrN and HfN are given in Table 4, along with the experimental [3] and theoretical data [8,11,29-30]. Obviously, the calculated results are in accordance with the experimental data [3] and previous theoretical results [8, 11, 29-30].

For a stable hexagonal structure, the five independent elastic constants C_{ij} ($C_{11}, C_{12}, C_{33}, C_{13}, C_{44}$) should satisfy the well known Born-Huang criteria for stability [31].

$$C_{12} > 0, C_{33} > 0, C_{11} > C_{12}, C_{44} > 0$$

$$(C_{11} + C_{12})C_{33} > 2C_{13}^2$$

while for a cubic crystal, the three independent elastic constants C_{ij} (C_{11}, C_{12}, C_{44}) should satisfy the Born-Huang criteria for the stability of cubic crystals [31].

$$C_{44} > 0, C_{11} > |C_{12}|, C_{11} + 2C_{12} > 0$$

The calculated elastic constants C_{ij} (GPa) satisfy these conditions, ensuring the mechanical stability of ZrN and HfN at ambient pressure. Young's modulus (E) and Poisson's ratio ν are the two important factors for technological and engineering application. The stiffness of the solid can be analyzed using the young's modulus (E) value. The Young's modulus (E) and Poisson's ratio ν are calculated using the following formulae

$$E = \frac{9BG}{(3B+G)} \quad (4)$$

$$\nu = \frac{(3B-2G)}{2(3B+G)} \quad (5)$$

Among the phases considered for ZrN and HfN, cubic B1 phase is stiffer than the other phases (B2, B3, Bh, and B8). During elastic deformation no volume change occurs, If

Table 4: Calculated elastic constants C_{ij} (GPa), bulk modulus B_0 (GPa) and its derivative B_0' , Young's modulus E (GPa), shear modulus G (GPa), Poisson's ratio, B/G ratio, Elastic anisotropy A , and microhardness H (GPa) for five different phases of ZrN and HfN.

| | ZrN | | | | | HfN | | | | |
|----------|------------------|------------------|------------------|------------------|------------------|------------------|------------------|------------------|------------------|-------|
| | B1 | B2 | B3 | Bh | B8 | B1 | B2 | B3 | Bh | B8 |
| C_{11} | 550 | 475 | 259 | 417 | 407 | 673 | 523 | 315 | 450 | 394 |
| | 471 ^a | 478 ^b | 261 ^b | 417 ^c | 408 ^c | 679 ^a | 518 ^e | 303 ^e | 440 ^e | |
| | 530 ^b | | | | | 591 ^d | | | | |
| C_{12} | 100 | 100 | 144 | 137 | 116 | 122 | 117 | 155 | 170 | 102 |
| | 138 ^a | 98 ^b | 139 ^b | 136 ^c | 115 ^c | 119 ^a | 117 ^e | 163 ^e | 172 ^e | |
| | | | | | | 121 ^c | | | | |
| C_{44} | 108 | 58 | 75 | 70 | 73 | 126 | 85 | 79 | 102 | 100 |
| | 88 ^a | 34 ^b | 62 ^b | 69 ^c | 74 ^c | 150 ^a | 14 ^e | 77 ^e | 103 ^e | |
| | 110 ^b | | | | | 118 ^d | | | | |
| C_{13} | | | | 85 | 127 | | | | 107 | 231 |
| | | | | 85 ^c | 130 ^c | | | | 109 ^e | |
| C_{33} | | | | 602 | 510 | | | | 645 | 425 |
| | | | | 599 ^c | 520 ^c | | | | 645 ^e | |
| B_0 | 250 | 225 | 182 | 228 | 229 | 306 | 253 | 208 | 257 | 247 |
| | 215 ^a | 225 ^b | 179 ^b | 225 ^c | 228 ^c | 306 ^a | 251 ^e | 210 ^e | 253 ^e | |
| | 250 ^b | | | | | 279 ^d | | | | |
| B_0' | 4.28 | 4.19 | 4.04 | 4.08 | 4.19 | 4.12 | 4.10 | 4.02 | 4.09 | 4.18 |
| E | 376 | 281 | 181 | 329 | 308 | 463 | 337 | 210 | 368 | 203 |
| G | 154 | 109 | 68 | 131 | 121 | 186 | 132 | 79 | 146 | 116 |
| ν | 0.24 | 0.29 | 0.33 | 0.25 | 0.27 | 0.24 | 0.27 | 0.33 | 0.26 | 0.29 |
| B/G | 1.62 | 2.06 | 2.67 | 1.74 | 1.89 | 1.64 | 1.91 | 2.63 | 1.76 | 2.12 |
| A | 0.33 | 0.30 | 0.372 | - | - | 0.31 | 0.26 | 0.33 | - | - |
| H | 26.27 | 15.24 | 7.71 | 21.93 | 18.59 | 32.17 | 20.34 | 9.00 | 23.24 | 15.89 |

^a Exp, Ref. [3].^b GGA, Ref. [8].^c Ref. [29].^d US-PP within GGA, Ref. [30]^e US-PP, Ref. [11].

$\nu = 0.5$, this indicates that the material is incompressible. The low ν value means that a large volume change is associated with its deformation. In addition, Poisson's ratio provides more information about the characteristics of the bonding forces than any of the other elastic constants. Among the five different phases of ZrN and HfN, the Poisson's ratio of cubic B1 phase is lower than other phases (B2, B3, Bh and B8), indicating that Zr-N and Hf-N bonding are more directional in the B1 phase. In order to predict the brittle and ductile behavior of solids, Pugh [32] introduced a simple relationship that the ratio of bulk modulus to shear modulus (B/G) is associated with ductile or brittle characters

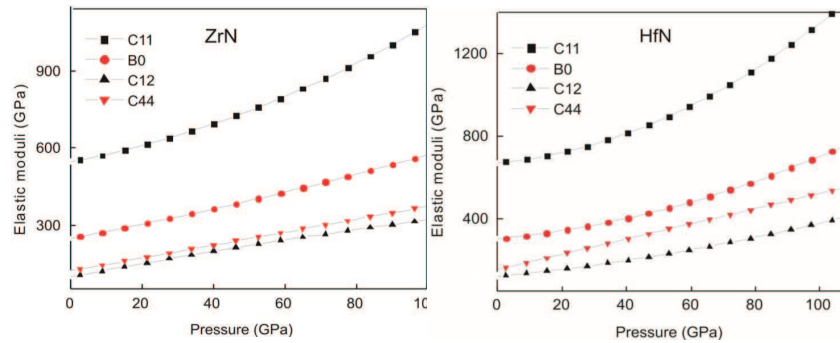


Figure 4: Calculated pressure dependence of elastic constants C_{ij} and bulk modulus B_0 (GPa) B1- ZrN and B1-HfN at $T=0$ K.

of a material. A high B/G corresponds to ductility, whereas a low ratio is associated with brittleness. Pugh [32] gave a critical value for ductile-brittle transition.

If $B/G < 1.75$, the material behaves in a brittle manner, otherwise, in a ductile manner. At 0 K and 0 GPa, the calculated values for ZrN and HfN shows that these materials are brittle for B1 phase and ductile for B2,B3,Bh and B8 Phases. This conclusion is in accordance with theoretical results [29,33] and experimental data[3]. Generally all crystals are elastically anisotropic, even a cubic crystal, which is isotropic in structure, has elastic anisotropy as a result of a fourth rank tensor property of elasticity. A proper description of an anisotropic behavior has a very important implication in engineering science as well as in crystal physics. For a cubic crystal, the elastic anisotropic parameter A is given by

$$A = \frac{2C_{44}}{(C_{11} + C_{12})} \tag{6}$$

For elastically isotropic crystals, anisotropic parameter A must be equal to one, while any departure from unity corresponds to the degree of elastic anisotropy possessed by the crystal. Our calculated the anisotropic parameter A for B1-ZrN and B1-HfN at 0 GPa is 0.33, which is in good agreement with theoretical value 0.53 [29]. The calculated pressure dependence of elastic constants C_{ij} (GPa) and bulk modulus of B1 phase ZrN and HfN are shown in Fig. 4.

From these figures, it is observed that C_{11} varies largely under the effect of pressure as compared with the variations in C_{12} and C_{44} . The elastic constant C_{11} represents the elasticity in length. A longitudinal strain produces a change in C_{11} . The elastic constants C_{12} and C_{44} are related to the elasticity in shape, which is a shear constant. A transverse strain causes change in shape without change in volume. Therefore, C_{12} and C_{44} are less sensitive to pressure as compared with C_{11} . As pressure increases all the elastic constants and bulk modulus of B1 phase of ZrN and HfN increases monotonically. The investigation of the stiffness can be completed by providing the micro hardness parameter H ,

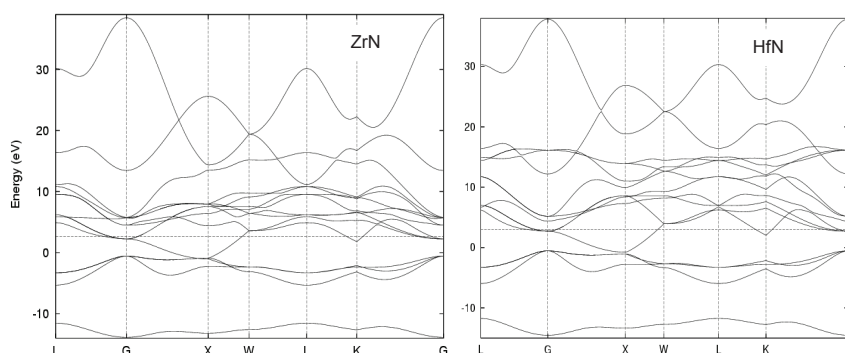


Figure 5: Band structure of (a) ZrN and (b) HfN in NaCl structure at normal pressure.

given by the following relation [34]

$$H = \frac{(1-2\nu)E}{6(1+\nu)} \quad (7)$$

The calculated H values are given in Table 4 reveals that HfN is harder than ZrN due to the strong covalent-ionic Hf-N bonds.

3.3 Electronic structure

The normal pressure band structure of ZrN and HfN along the symmetry directions L- Γ -X-W-L (for NaCl structure) are given in Fig. 5(a) and (b) respectively. The Fermi level is indicated by dotted horizontal line.

The overall topology of the band structure under normal pressure is same for both ZrN and HfN. From the band structure of ZrN (Fig. 5a) and HfN (Fig. 5b), it is evident that the lowest band lying around -12 eV is mainly due to N-2s states. The energy bands, which lies around -5 eV arise mainly from Zr-5s (Fig. 5a) and Hf-6s (Fig. 5b) and also contain a small contribution from 2p state electrons of the nitrogen atom. The Zr-4d and Hf-5d like bands at the Fermi level hybridize with N-2p states and lie together at the X point. There is no energy gap between the conduction band and the valence band. Hence at normal pressure both ZrN and HfN exhibit metallic character. The total density of states of ZrN and HfN in the NaCl, ZB, CsCl, WC and NiAs structure are given in Fig. 6 (a-b) respectively.

In the density of states of ZrN and HfN with NaCl structure, there is a deep valley called pseudo gap near the Fermi level which results from the strong hybridization between nd ($n = 4,5$) states of the transition metal atom (TM=Zr,Hf) and N-2p states. The presence of pseudo gap indicates significant covalent bonding between TM and N atoms in the cubic NaCl structure. In addition the energy region for the hybridization between the transition metal (TM=Zr,Hf) nd ($n = 4,5$) states and N-2p states in the NaCl structure is from -8 to 0 eV for ZrN and -10 to 0 eV for HfN, which is wider than those in another

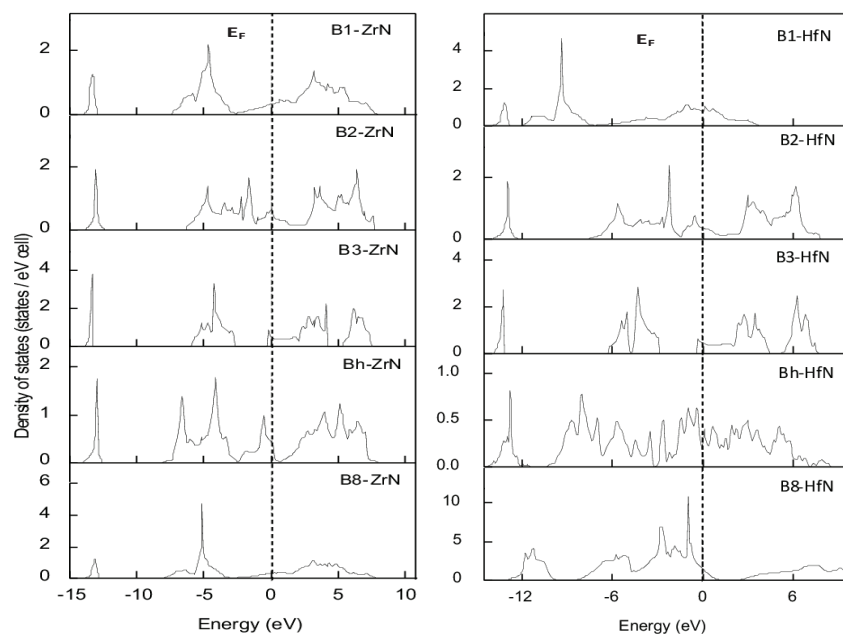


Figure 6: Total density of states of (a) ZrN and (b) HfN in five different phases. The Fermi level is indicated as dotted lines.

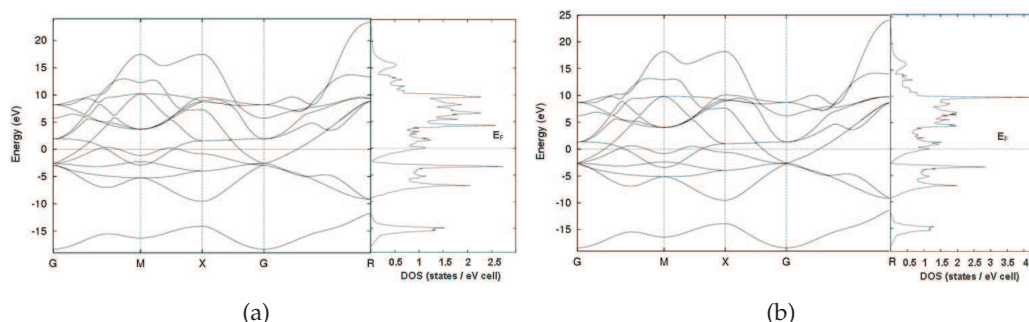


Figure 7: High pressure band structure and density of states of : (a) ZrN and (b) HfN in the CsCl structure.

structures (CsCl, ZB, WC and NiAs) and hence suggest the TM-N (TM=Zr,Hf) bonding in the NaCl structure exhibit characteristics. From Fig. 6, it is found that the density of states at the Fermi level in the NaCl structure in the other structures. This indicates that both ZrN and HfN have higher conductivity in NaCl structure.

Under high pressure, ZrN and HfN undergo structural phase transition from sixfold coordinated NaCl structure to eightfold coordinated CsCl structure. So for computing the high pressure band structure and density of states, we have chosen the CsCl structure as the stable structure for ZrN and HfN (Fig. 7).

As pressure increases, the entire band structure is slowly shifted up in energy and the

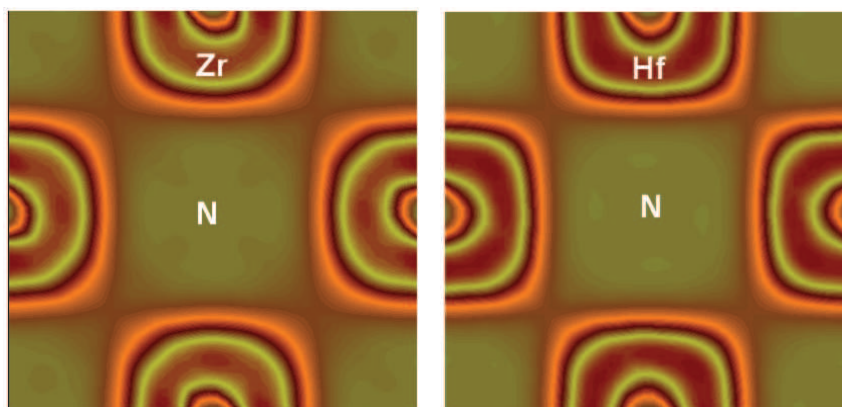


Figure 8: Charge density distribution of cubic B1 phase of: (a) ZrN (b) HfN.

valence band width increases. This is because of the enhanced overlapping of the wave functions with the neighboring atoms. Visible changes are seen in the band structure at Γ point corresponding to high pressure structure (Fig. 7), Since the electronic system is strongly coupled to the lattice under pressure.

To visualize the nature of the bond character, charge density distribution of cubic NaCl phase of ZrN and HfN are shown in Fig. 8. From these figures, it is observed that there is an increase of the electron density around the N atoms, and a decrease in the interstitial region between the transition metal atoms (TM=Zr,Hf) where the metal-metal bonds have formed. We note the difference of the electronegativities between the transition metal (TM-Zr,Hf) and N appears in the difference of charge transfer. These imply that beside the strong covalent interaction, an ionic contribution also exists in the Zr-N and Hf-N systems. Therefore, the bonding is a unusual mixture of metallic, covalent and ionic in attribution in ZrN and HfN.

3.4 Superconductivity under pressure

Hard superconducting materials are of considerable interest for specific applications. Transition metal nitrides having sodium chloride structure (e.g VN, NbN) are also hard superconductors with relatively higher T_c . The continuous promotion of s, p to d shell in solids under pressure is one of the factor which will induce superconductivity. The superconducting transition temperature (T_c) is calculated using the Allen dynes formula [35]

$$T_c = \frac{\langle \omega \rangle}{1.2} \exp \left[\frac{-1.04(1+\lambda)}{\lambda - \mu^*(1+0.62\lambda)} \right] \quad (8)$$

where $\langle \omega \rangle$ is the average phonon frequency and is given by

$$\langle \omega \rangle = \sqrt{(0.5\theta_D^2)} \quad (9)$$

Table 5: μ^* , λ , $\langle \omega \rangle$ and T_c as function of pressure for ZrN and HfN in the normal pressure structure (NaCl structure).

| ZrN | | | | | HfN | | | | |
|--------------|---------|--------------------|--------------------------|-------------------|--------------|---------|-----------|--------------------------|--------------|
| P (GPa) | μ^* | λ | $\langle \omega \rangle$ | T_c (K) | P (GPa) | μ^* | λ | $\langle \omega \rangle$ | T_c (K) |
| 0.00 | 0.10 | 0.62 | 364 | 917 | 0.00 | 0.10 | 0.8 | 185 | 8.66 |
| | | 0.626 ^a | | 10.0 ^a | | | | | |
| 33.02 | 0.11 | 0.63 | 456 | 10.87 | 17.44 | 0.11 | 1.0 | 220 | 14.58 |
| 90.01 | 0.15 | 0.69 | 687 | 14.24 | 38.11 | 0.12 | 1.05 | 260 | 17.73 |
| 98.53 | 0.16 | 0.73 | 743 | 16.66 | 69.57 | 0.124 | 1.12 | 290 | 21.42 |
| 133 | 0.166 | 0.72 | 790 | 15.83 | 134 | 0.126 | 1.13 | 310 | 22.9 |
| 192 | 0.17 | 0.70 | 840 | 14.52 | 159 | 0.127 | 1.02 | 330 | 20.73 |

^a Ref. [3].

where θ_D is the debye temperature. The electron phonon coupling constant is calculated using the formula

$$\lambda = \frac{N(E_F) \langle I^2 \rangle}{M \langle \omega^2 \rangle} \quad (10)$$

where M is the atomic mass, $\langle \omega^2 \rangle$ is an average of the phonon frequency square and $\langle I^2 \rangle$ is the square of the electron-phonon matrix element averaged over the Fermi energy. The electron-electron interaction parameter is estimated using the relation

$$\mu^* = \frac{0.26N(E_F)}{(1+N(E_F))} \quad (11)$$

with the Fermi energy and $N(E_F)$ obtained from the self-consistent calculation. The calculated values of μ^* , $\langle \omega \rangle$, λ and T_c under various pressures for cubic NaCl zirconium nitride (ZrN) and hafnium nitride (HfN) are given in Table 5. As Debye temperature is proportional to the characteristic phonon frequency of the lattice. The path to higher T_c lies in the direction of higher $\theta_D(P)$. But under high pressure, a higher Debye temperature can also lower T_c . That is because the coupling constant can decrease, if the phonon frequencies are large. At normal pressure, the calculated T_c value is 9.17 K and 8.66 K for ZrN and HfN respectively. This is in good agreement with the experimental observation of Chen *et al.* [3]. In ZrN and HfN, the increase of T_c is due to increase of λ and delocalized anion d-electron number.

Phonon softening also enhances the superconducting transition temperature in zirconium nitride and hafnium nitride under high pressure. The contribution from $\mu^*(P)$ to the variation of $T_c(P)$ is much less than that of $\lambda(P)$. From this it is concluded that both ZrN and HfN are electron-phonon mediated superconductors. The $T_c(\text{max})$ value of ZrN and HfN in the NaCl (B1) structure is attributed due to N-3d state electrons. The decrease in T_c above 98.53 GPa in ZrN and 134 GPa in HfN is due to the phase transition from B1 to B2 phase.

4 Conclusions

We report, the electronic band structure, density of states, charge density distribution, mechanical properties, structural phase transition and superconducting transition temperature of ZrN and HfN under normal and high pressure. Our results suggest that at ambient pressure, ZrN and HfN are stable in the cubic NaCl structure. From our analysis, we also predict B1 to B2 phase transition in ZrN and HfN under pressure. The calculated bulk modulus values reveal that these materials are incompressible. It is observed that the bonding in cubic NaCl-ZrN and NaCl-HfN are a mixture of metallic, covalent, and ionic characters. At normal pressure, it is found that HfN is harder than ZrN. When the pressure is increased, it is predicted that, T_c increases and reaches a maximum value thereafter T_c starts to decrease. The main reason behind the decrease in T_c is the structural phase transition. The highest value of $T_c(P)$ estimated is 16.66 K for B1-ZrN and 22.9 K for B1-HfN.

Acknowledgments. We thank our college management for their constant encouragement. The financial assistance from UGC (MRP F.No.38-141/2009), India is duly acknowledged with thanks.

References

- [1] N. W. Ashcroft, Nature 419 (2002) 569.
- [2] A. Lindbaum, S. Heathman, K. Litfin, and Y. Meresse, Phys. Rev. B 63 (2001) 214101.
- [3] X. Chen, V.V. Struzhkin, Z. Wu, M. Somayazulu, J. Qian, S. Kung, A.N. Christensen, Y. Zhao, R.E. Cohen, H.-K. Mao, and R. J. Hemley, Proc. Natl. Acad. Sci. Am. 102 (2005) 3198.
- [4] A. F. Guillermet, J. Haglund, and G. Grimvall, Phys. Rev. B 45 (1992) 11557.
- [5] C. Stampfl, W. Mannstadt, R. Asahi, and A. J. Freeman, Phys. Rev. B 63 (2001) 155106.
- [6] E. I. Isaev, S. I. Simak, I. A. Abrikosov, R. Ahuja, Yu Kh Vekilov, M. I. Katsnelson, A. I. Lichtenstein, and . Johansson, J. Appl. Phys. 101 (2007) 123519.
- [7] P. Ojha, M. Aynyas, and S. P. Sanyal, J. Phys. Chem. Solids 68 (2007) 148.
- [8] Y. J. Hao, H. S. Ren, B. Zhu, J. Zhu, J. Y. Qu, and L. Q. Chen, Solid State Sci. 10.1016/j.solidstatesciences.2012.08.010.
- [9] M. Yamamoto, M. Kurahashi, C. T. Chan, K. M. Ho, and S. Naito, Surf. Sci. 387 (1997) 300.
- [10] S. Yamanaka, K. Hotehama, and H. Kawaji, Nature 392 (1998) 580.
- [11] E. Zhao and Z. Wu, J. Solid State Chem. 181 (2008) 2814.
- [12] P. Perdew, S. Burke, Phys. Rev. B 54 (2004) 16533.
- [13] P. E. Blöchl, Phys Rev B 50 (1994) 17953.
- [14] G. Kresse, J. Joubert, Phys Rev B 59 (1999) 1758.
- [15] G. Kresse and J. Hafner, Phys. Rev. B 47 (1993) 558.
- [16] G. Kresse and J. Furthmuller, Comp. Mater. Sci. 6 (1996) 15.
- [17] J. P. Perdew and S. Burke, Phys. Rev. Lett. 78 (1997) 1396.
- [18] H. J. Monkhorst and J. D. Pack, Phys.Rev.B 13 (1976) 5188.
- [19] H. L. Skriver, The LMTO Method (Springer, Heidelberg, 1984).
- [20] O. K. Anderson, Phys. Rev. B 12 (1975) 3060.
- [21] O. Jepsen and O. K. Anderson, Solid State Commun. 9 (1971) 1763.

- [22] F. D. Murnaghan, Proc. Natl. Acad. Sci. USA 30 (1944) 244.
- [23] J. F. Nye, Physical Properties of Crystals, Their Representation by Tensors and Matrices (Oxford Press, Oxford, 1957).
- [24] M. Kalay, H. H. Kart, and T. Cagin, J. Alloy. Com. 484 (2009) 431.
- [25] G. Steinle-Neumann, L. Stixrude, and R. E. Cohen, Phys. Rev. B 69 (2004) 219903.
- [26] W. Voigt, Lehrbuch de Kristallphysik (Terubner, Leipzig, 1928).
- [27] A. Reuss, Z. Angew. Math. Mech. 9 (1929) 49.
- [28] R. Hill, Proc. Phys. Soc., London, Sec. A 65 (1952) 349.
- [29] E. Zhao, J. Wang, J. Meng, and Z. Wu, Comp. Mater. Sci. 47 (2010) 1064.
- [30] S. Nagao, K. Nordlund, R. Nowak, Phys. Rev. B 73 (2006) 144113.
- [31] M. Born and K. Huang, Dynamical Theory of Crystal Lattices (Clarendon, Oxford, 1956).
- [32] S. F. Pugh, Philos. Mag. 45 (1954) 823.
- [33] W. Chen and J. Z. Jiang, J. Alloy. Comp. 499 (2010) 243.
- [34] N. H. Miao, B. S. Sa, J. Zhou, and Z. M. Sun, Comp. Mater. Sci. 50 (2011) 1559.
- [35] P. B. Allen and R. C. Dynes, Phys. Rev. B 12 (1975) 905.